

Defects in Mitochondrial Fission Protein Dynamin-Related Protein 1 Are Linked to Apoptotic Resistance and Autophagy in a Lung Cancer Model

Kelly Jean Thomas^{1,2*}, Marty R. Jacobson²

1 Biological Sciences Department, Colorado Mesa University, Grand Junction, Colorado, United States of America, **2** Saccomanno Research Institute, St. Mary's Hospital and Regional Medical Center, Grand Junction, Colorado, United States of America

Abstract

Evasion of apoptosis is implicated in almost all aspects of cancer progression, as well as treatment resistance. In this study, resistance to apoptosis was identified in tumorigenic lung epithelial (A549) cells as a consequence of defects in mitochondrial and autophagic function. Mitochondrial function is determined in part by mitochondrial morphology, a process regulated by mitochondrial dynamics whereby the joining of two mitochondria, fusion, inhibits apoptosis while fission, the division of a mitochondrion, initiates apoptosis. Mitochondrial morphology of A549 cells displayed an elongated phenotype—mimicking cells deficient in mitochondrial fission protein, Dynamin-related protein 1 (Drp1). A549 cells had impaired Drp1 mitochondrial recruitment and decreased Drp1-dependent fission. Cytochrome c release and caspase-3 and PARP cleavage were impaired both basally and with apoptotic stimuli in A549 cells. Increased mitochondrial mass was observed in A549 cells, suggesting defects in mitophagy (mitochondrial selective autophagy). A549 cells had decreased LC3-II lipidation and lysosomal inhibition suggesting defects in autophagy occur upstream of lysosomal degradation. Immunostaining indicated mitochondrial localized LC3 punctae in A549 cells increased after mitochondrial uncoupling or with a combination of mitochondrial depolarization and ectopic Drp1 expression. Increased inhibition of apoptosis in A549 cells is correlated with impeded mitochondrial fission and mitophagy. We suggest mitochondrial fission defects contribute to apoptotic resistance in A549 cells.

Citation: Thomas KJ, Jacobson MR (2012) Defects in Mitochondrial Fission Protein Dynamin-Related Protein 1 Are Linked to Apoptotic Resistance and Autophagy in a Lung Cancer Model. PLoS ONE 7(9): e45319. doi:10.1371/journal.pone.0045319

Editor: Janine Santos, University of Medicine and Dentistry of New Jersey, United States of America

Received: April 10, 2012; **Accepted:** August 20, 2012; **Published:** September 20, 2012

Copyright: © 2012 Thomas, Jacobson. This is an open-access article distributed under the terms of the Creative Commons Attribution License, which permits unrestricted use, distribution, and reproduction in any medium, provided the original author and source are credited.

Funding: St. Mary's Hospital and Regional Medical Center, St. Mary's Hospital Foundation. The funders had no role in study design, data collection and analysis, decision to publish, or preparation of the manuscript.

Competing Interests: The authors have declared that no competing interests exist.

* E-mail: kjcraig@coloradomesa.edu

Introduction

Cancer is a major public health problem around the world. Current strategies in cancer therapy (chemo- and radiotherapy) rely on killing tumor cells by mechanisms largely mediated by the activation of apoptosis. Apoptosis is a conserved cellular process that controls normal development and tissue homeostasis by eliminating damaged cells. Inhibition of apoptosis contributes to the tumorigenic conversion of normal cells by extending their viability, favoring the accumulation of transforming mutations [1]. Resistance to apoptosis is linked to increased invasive and metastatic potential in cancer cells [2].

A classic cancer hallmark is apoptotic resistance [3]. How tumor cells evade apoptotic cell death is currently unknown, but increasing tumor sensitivity to apoptosis is a therapeutic goal. The absence of spontaneous apoptosis and treatment-induced apoptosis in non-small cell lung cancer (NSCLC) suggests that deficiencies in the apoptotic process may be responsible for their resistance to anti-cancer therapy [4]. Gene mutations and altered expression of apoptosis regulators are detected in lung cancer. Differences in sensitivity to therapeutics that induce apoptosis may be related to the expression of apoptosis regulators in lung cancer. Anti-apoptotic modulating therapy is being extensively investigated [3].

Intrinsic apoptosis is characterized by permeabilization of mitochondria, release of cytochrome c, and activation of the caspase cascade [5]. Mitochondrial control of apoptosis occurs upstream of caspase activation and is mediated by the Bcl-2 family of proteins [5]. Bcl-2 proteins also influence mitochondrial dynamics, a process that balances mitochondrial fission and fusion events to regulate the shape, structure and function of the mitochondrion [5]. Mitochondria are dynamic organelles whereby their shape corresponds to the metabolic status [6], the health of the cell [7] and balance between fusion and fission is required for homeostasis. Normally, mitochondrial fission mediator Drp1 fragments mitochondria [5]. Drp1 is a large GTPase that controls membrane tubulation and fission in mammalian cells [5]. Cells undergoing mitochondrial fission will have shorter mitochondrial length when compared to cells that are undergoing mitochondrial fusion [8]. Although these events are transient, cells deficient in a mitochondrial dynamics protein or under stimuli will maintain their state-dependent mitochondrial morphology [6]. Excessive mitochondrial fission (fragmentation) is essential for intrinsic apoptosis—it is necessary for cytochrome c release and subsequent caspase activation [5].

Inhibition of Drp1-dependent mitochondrial fission impairs and partially inhibits intrinsic apoptosis [7]. Concomitant with

mitochondrial membrane permeabilization during apoptosis, Drp1 forms oligomers and is recruited to the outer mitochondrial membrane to mediate fission in a GTP-dependent manner [5]. Fission events mediate apoptosis by regulating the release of pro-apoptotic factors to the cytosol. Inhibition of Drp1 prevents mitochondrial membrane potential collapse and cytochrome c release, and promotes elongated mitochondrial morphological phenotypes [5]. Inhibition of mitochondrial fission prohibits cytochrome c translocation and delays cell death, thus providing a link between mitochondrial dynamics and the induction of apoptosis.

Mitochondrial dynamics not only impact intrinsic apoptosis, but also redirect autophagic degradation. Extensive cross-talk exists between mitophagy and apoptosis [9]. Inhibition of fission mediators such as Dynamin-related protein 1 (Drp1), which impairs intrinsic apoptosis [10], has been shown to decrease mitophagy [11]. Downregulation of autophagy during tumor progression has been noted in many studies [12]. Increased tumorigenicity has been shown to decrease protein degradation in lung epithelial cells [13]. The negative regulator of autophagy, mTOR (mammalian target of rapamycin), is frequently activated [14] and mTOR inhibitors have been shown to limit tumor proliferation in NSCLC models [15].

Resistance to apoptosis is linked to mitochondria and proteins involved in mitochondrial dynamics. However, it remains unknown if tumor cells gain resistance to apoptosis by altering mitochondrial dynamics. In this study, we characterized mitochondrial dynamics and the downstream process of apoptosis in lung cancer cells. Differences in mitochondrial morphology and function were observed in A549 cells. We provide evidence in lung cancer cells suggesting an imbalance in mitochondrial dynamics exists, whereby defects in Drp1-dependent mitochondrial fission inhibit the downstream process of autophagy and contribute to apoptotic resistance.

Materials and Methods

Cell Culture and Plasmids

Cell lines purchased from ATCC (Table I) were cultured as described previously [16]. Live cell imaging was performed in phenol red free (PRF) OptiMEM (Invitrogen). Plasmids [16] for mitochondrial YFP (mito-YFP, Clontech), Drp1-YFP [17], Drp1-myc [18], Drp1 K38A-myc [18], and Drp1 RNAi [19] were gifts from Dr. Richard Youle (NINDS, Bethesda, MD) and were transfected into cells using Lipofectamine 2000 (Invitrogen) as directed by the manufacturer. Plated cells (10^4 cells/well) were seeded and cultured in complete OptiMEM for 24 hours at 37°C, prior to treatment and fluorescent intensity reading. Cells treatment included: Incubation with 1 μ M staurosporine (STS, Sigma) and/or 50 μ M zVAD-FMK (Sigma) for 3 hours in PRF OptiMEM without serum in apoptotic assays. Cells were starved

using EBSS (Invitrogen) and/or treated with 10 nM Bafilomycin A1 (Sigma) for 24 hours in autophagy assays.

Analysis of Mitochondrial Morphology and Connectivity

Mitochondrial morphology was analyzed as previously described [16] using live cell imaging with an inverted confocal microscope (CARV spinning disk, DMI 6000B, Leica) and MetaMorph software. Mitochondrial length analysis was performed on images using ImageJ after processing to find edges. The average mitochondrial length was determined after using the freehand line selection tool to measure length (micrometers) of individual mitochondria obtained in a randomly selected field of 100×100 pixels and 10–15 cells per cell line were examined. Associated metadata were displayed and the image scale (Distance in Pixels: 1; Known Distance: Value from Metadata; Pixel Aspect Ratio: 1; Unit of Length: micrometer; Global: checked) was set for image analysis consistency. Transient cell transfection and Drp1 RNAi knockdown experiments were performed as described [16]. Mitochondrial imaging with 0.5 μ g transfected mito-YFP or mito-DsRED, mitochondrial length estimates and mitochondrial FRAP assays have been described [16,20].

Cellular Imaging and Fluorimetry

Mitochondrial mass was estimated using a fluorescent plate reader after staining cells with 200 nM Mitotracker Green for 30 minutes at 37°C, and washing once with PRF-OptiMEM [21]. Fluorescence intensity measurements reported are background subtracted (495/515 nm).

Mitochondrial membrane potential was estimated in a 96-well plate using a fluorescent plate reader (Tecan). Cells (10^4 per well) were loaded with 10 nM TMRE for 30 minutes at 37°C in normal growth media. The TMRE loading medium was removed and cultures were placed in phenol red free, serum free media and incubated for an additional 15 minutes to allow for the TMRE fluorescent signal to reach steady state. Fluorescence intensity was then captured 1/min for 5 minutes to establish a baseline. After 5 minutes, 6 μ M oligomycin (Cell Signaling) was added to induce hyperpolarization of $\Delta\Psi_m$. In the presence of oligomycin, 10 μ M CCCP was added at 18 minutes to the cells to cause depolarization of the $\Delta\Psi_m$. TMRE expression is plotted as a relative ratio $\Delta F/F_0$ showing mean and SEM, where F indicates fluorescence intensity and F_0 indicates baseline values before stimulation. All cell lines analyzed displayed oligomycin-induced hyperpolarization of mitochondrial membrane potential. Fluorescence intensities are background subtracted (554/576 nm).

Mitophagy was measured using confocal microscopy to detect colocalization of mito-YFP transfected positive cells with immunostaining against mouse monoclonal anti-LC3B (Novus Biologicals) with AlexaFluor® 594 secondary anti-mouse IgG antibody (Invitrogen). Cells (5×10^4 per well) were transfected in suspension with 0.5 μ g mito-YFP using Lipofectamine 2000 (Invitrogen) and seeded on LabTekII borosilicate glass chambers (Nunc) for 24 h.

Table 1. Lung epithelial cell lines used.

Designation	ATCC #	Tissue	Disease	Tumor type	Tumorigenic (Ref)
NL20	CRL-2503	bronchis	normal	N/A	No [49]
NL20TA	CRL-2504	bronchis	normal	N/A	Yes, weakly [49]
Calu1	HTB-54	lung	squamous cell carcinoma	pleural metastasis	Yes [50]
A549	CCL-185	alveolar	adenocarcinoma	1° explant lung culture	Yes [51]

doi:10.1371/journal.pone.0045319.t001

After fixation with 4% paraformaldehyde, cells were immunostained with rabbit polyclonal anti-LC3B antibody (Novus Biologicals) and visualized with AlexaFluor® 594 goat anti-rabbit IgG (590/617 nm). The number of distinct mitochondria localized LC3-positive punctae per cell was counted. Autophagosome formation was noted by LC3 punctae.

All fluorescence measurements have relative fluorescence units (RFU).

ELISA, Phosphoprotein Purification and Western Blotting

General methods for western blotting and subcellular fractionation have been described [20]. Antibodies used: Sigma (β -actin, GAPDH), Cell Signaling (caspase-3, HSP60, HTRA2, PARP), BD Translabs (Drp1, p53, TIM23), Calbiochem (VDAC), Novus (LC3-II), Abcam (vimentin, fibronectin) and MitoSciences (Mitochondrial Assay, complex IV subunit I, frataxin). The antibody against Drp1 pS637 was a generous gift from Dr. Craig Blackstone (NINDS, Bethesda, MD). Phosphoprotein purification was performed as previously described [16].

Statistics

Tests for analysis are indicated in the figure legend and significance is denoted as follows: ns, not significant $P > 0.05$; * $P < 0.05$; ** $P < 0.01$; *** $P < 0.001$.

Results

Mitochondrial Elongation in A549 Cells

Mitochondrial dysfunction has been observed in many types of cancer cell lines [22]. An important determinant of mitochondrial function is mitochondrial morphology. Mitochondrial morphology was examined in each of our normal and lung cancer cell lines (Table 1) using a mito-YFP to fluorescently label the mitochondrial matrix of cells (Figure 1A). Mitochondrial length was also determined for each cell line (Figure 1B). Distinct differences in the morphology, including the length of mitochondria, were observed between lung epithelial cell lines that vary in tumorigenic potential (Table 1) and relative tumorigenic potential of each cell line was validated after performing cell migration experiments (Figure S1) [23]. The non- and weakly tumorigenic NL20 and NL20TA cells had a heterogeneous phenotype but the tumorigenic Calu1 and A549 cells displayed predominantly the elongated form of mitochondria. A trend was noted whereby the non-tumorigenic cells (NL20) had the shortest mean mitochondrial length (mean \pm SEM; $5.2 \pm 0.4 \mu\text{m}$) and the longest mean mitochondrial length was observed in A549 cells (mean \pm SEM; $8.0 \pm 0.8 \mu\text{m}$) (Figure 1).

Increased Mitochondrial Mass in A549 Cells

Mitochondrial mass was estimated in live cells using Mitotracker Green FM, which accumulates in mitochondria regardless of mitochondrial membrane potential [24]. After normalization for cell volume, it was observed that A549 cells had increased mitochondrial mass compared to the other lung epithelial cell lines (Figure 2A). To further validate this relationship, the expression of a mitochondrial encoded protein, mitochondrial complex IV subunit I (the terminal enzyme of the respiratory chain) was compared to nuclear encoded mitochondrial-associated proteins, TIM23 (translocase of the inner mitochondrial membrane 23) and frataxin by two independent methods, immunoblot and ELISA (Figure 2B,D; respectively). A549 cells had increased levels of complex IV subunit I protein when compared to NL20 cells (Figure 2B–E). The selective accumulation of mitochondria in A549 cells was not mimicked by other organelles upon analysis of

protein expression (ER, calnexin; golgi, syntaxin 6; cytosol, GAPDH) by western blot (data not shown). Additionally, mitochondrial biogenesis markers TFAM (mitochondrial transcription factor A) and PGC1 α (peroxisome proliferator-activated receptor gamma coactivator-1 alpha) were examined to further investigate mitochondrial mass in the cell lines. Examination of these markers at the gene expression level does not suggest that increases in mitochondrial mass observed in A549 cells are attributed to increased mitochondrial biogenesis. Gene expression fold change differences were not significant in both gene evaluations (TFAM, $P < 0.142$; PGC1 α , $P < 0.119$) (data not shown). These data show A549 cells have increased mitochondrial mass.

Resistance to CCCP-induced Mitochondrial Depolarization in A549 Cells

Mitochondrial uncoupling by CCCP (carbonyl cyanide *m*-chloro phenyl hydrazone) disrupts mitochondrial membrane potential ($\Delta\psi_m$) and mitochondrial pH gradient (ΔpH_m) [20]. TMRE expression is plotted as a relative ratio, $\Delta F/F_0$, where F indicates fluorescence intensity and F_0 indicates baseline values before stimulation. All cell lines analyzed displayed oligomycin-induced hyperpolarization of mitochondrial membrane potential. In the presence of oligomycin, 10 μM CCCP was then added to the cells to cause depolarization of the $\Delta\psi_m$.

Our data suggest that A549 cell lines do not depolarize to the level of the other cell lines following CCCP treatment. Significant differences ($P < 0.001$; 2-way ANOVA) in $\Delta F/F_0$ are observed from 23–30 minutes (> 4 min after CCCP addition) between A549 and the other cell lines. This suggests that highly tumorigenic A549 cells display a resistance to mitochondrial membrane depolarization (Figure 3).

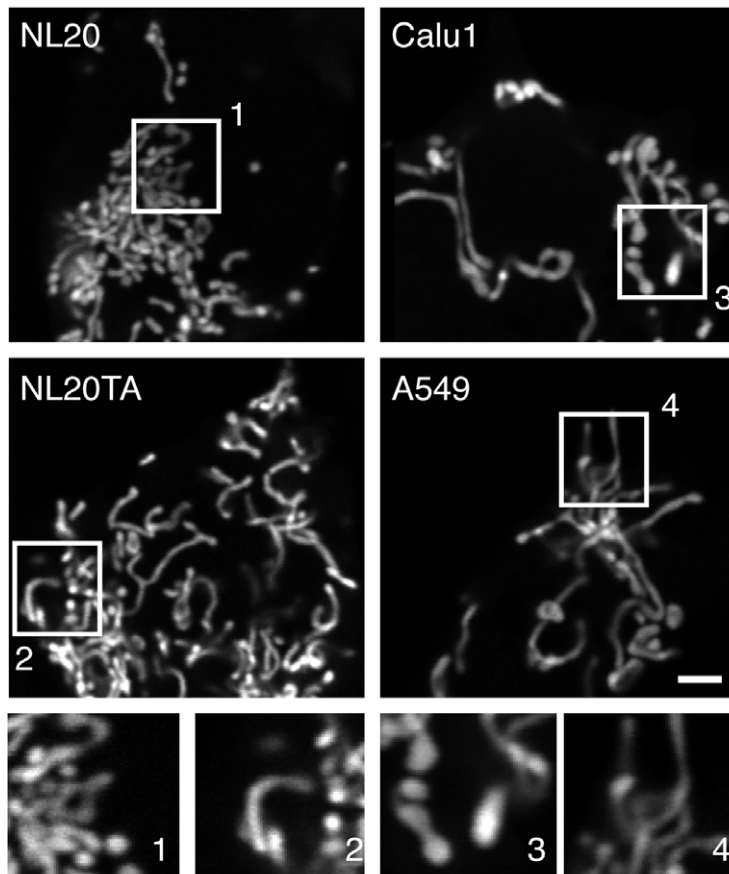
As tumor cell lines have previously been shown to be influenced by multidrug resistance transporters (MDR), cells were pre-treated with 50 μM verapamil to block MDR activity during TMRE loading to determine if MDR proteins in the plasma membrane had an effect on TMRE influx. Following oligomycin/CCCP treatment of verapamil treated cells, MDR did not influence the intracellular accumulation of TMRE when compared to non-verapamil treated cells (data not shown); as this fluorescent rhodamine substrate does not accumulate in drug resistant cells. In this study, A549 cells had less change in $\Delta\psi_m$ as measured by TMRE fluorescence following CCCP treatment and MDR activity does not influence this activity. These data are consistent with other reports that suggest cancer cells demonstrate resistance to mitochondrial membrane depolarization [25].

Decreased Drp1-dependent Fission in A549 Cells

Mitochondrial depolarization and fission are a prerequisite for intrinsic apoptosis [5]. With increased mitochondrial length, we hypothesized that A549 cells would have decreased mitochondrial fission, which would decrease both apoptotic initiation and the downstream catabolic process of autophagy.

Drp1 and its mitochondrial fusion antagonists Opal (Optic atrophy 1), Bax/Bak and Mfn1/2 (Mitofusin 1/2), in part, regulate the shape, structure and function of the mitochondria by mitochondrial dynamics [8]. Examination of mitochondrial morphology (Figure 1A; Figure 4A, basal) shows mainly elongated mitochondria in A549 cells (Figure 4A2: mitochondrial length, mean \pm SEM; $8.3 \pm 0.8 \mu\text{m}$). This phenotype suggests defects in fission or an upregulation of fusion. Steady state Drp1 protein levels were analyzed by immunoblot (Figure 4B,C). Quantitative analysis shows that basal Drp1 protein expression in A549 cells was at most 44% that observed in NL20 cells (Figure 4D).

A



B

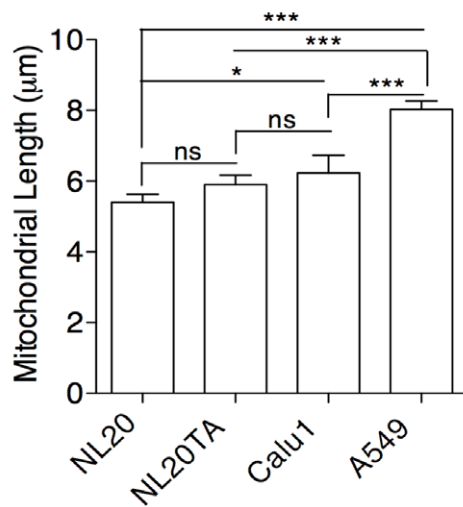


Figure 1. Mitochondrial length of lung epithelial cells. (A) Representative mito-YFP expression in cells. Numbered boxes (1–4) are magnifications (10 \times) of the corresponding numbered boxed regions in the original images of NL20, NL20TA, Calu1 and A549. Scale bar is 2 μ m. (B) Mean mitochondrial length (y-axis; \pm SEM) measurements ($n = 35$ – 50) from three independent experiments for NL20, NL20TA, Calu1, and A549 cells. 1-way ANOVA analysis with Tukey post-tests ($P < 0.0001$). doi:10.1371/journal.pone.0045319.g001

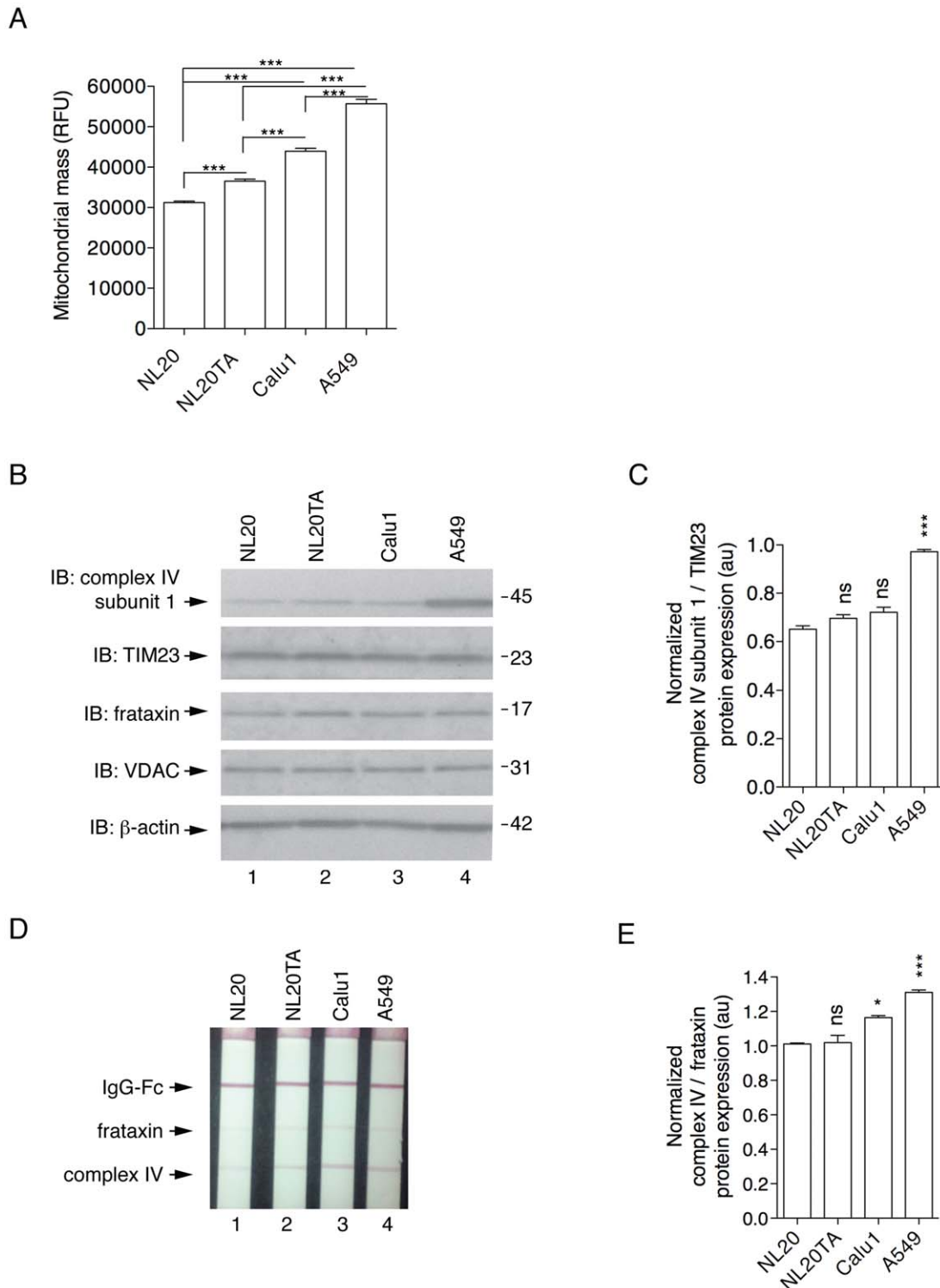


Figure 2. Mitochondrial mass of lung epithelial cells. (A) Mitotracker green fluorescence relative fluorescence units (y-axis, RFU) represents mitochondrial mass (mean and SEM); measurements ($n=8$ wells) from three independent experiments. 1-way ANOVA analysis with Tukey post-tests ($P<0.0001$). (B) Representative immunoblots demonstrating expression of endogenous proteins complex IV subunit I, TIM23, frataxin, and VDAC in NL20 (lane 1), NL20TA (lane 2), Calu1 (lane 3), and A549 (lane 4) cells. β -actin is shown for loading. Markers in kilodaltons (kDa). (C) Immunoblots from two independent experiments were quantified to show relative complex IV subunit I protein expression normalized to TIM23. Mean and SEM shown. 1-way ANOVA analysis with Tukey post-tests compared to NL20. (D) Representative mitochondrial biogenesis dipstick ELISA assay showing frataxin and complex IV expression. (E) Three independent mitochondrial biogenesis ELISA assays were quantified to show relative mitochondrial-encoded complex IV protein expression normalized to the nuclear-encoded frataxin protein. Mean and SEM shown. 1-way ANOVA analysis with Tukey post-tests compared to NL20.

doi:10.1371/journal.pone.0045319.g002

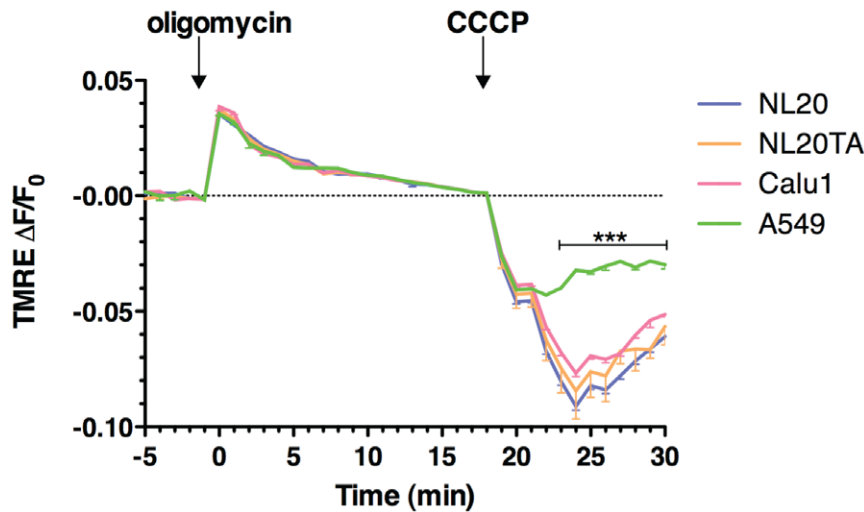


Figure 3. Resistance to mitochondrial uncoupling. TMRE staining from two independent experiments ($n=8$). TMRE expression is plotted as a relative ratio $\Delta F/F_0$ showing mean and SEM, where F indicates fluorescence intensity and F_0 indicates baseline values before stimulation following background subtraction. Cell lines NL20 (blue), NL20TA (orange), Calu1 (pink) and A549 (green) were treated with oligomycin ($6 \mu\text{M}$; 0 minutes) and CCCP ($10 \mu\text{M}$; 18 minutes) to induce hyperpolarization and depolarization, respectively. 2-way ANOVA analysis with Bonferroni post-tests. doi:10.1371/journal.pone.0045319.g003

To further manipulate mitochondrial morphology, Drp1 was knocked down using RNAi [16,19](Figure 4A,B +Drp1 RNAi), which is expected to elongate mitochondria. After Drp1 RNAi mediated knock down in NL20 and A549 cells, there was a robust decrease in Drp1 protein levels (Figure 4B,D). Mitochondrial length increased, as expected, in NL20 cells after Drp1 RNAi treatment (Figure 4A: mean \pm SEM; basal (A1), $4.9\pm 0.5 \mu\text{m}$; Drp1 RNAi (A3), $7.8\pm 0.6 \mu\text{m}$; 1-way ANOVA, Tukey post-test, $P<0.001$). The mitochondrial phenotype after Drp1 RNAi treatment in A549 cells was swollen and bulbous (Figure 4A4); a morphology caused by hyperfusion of the mitochondria due to a lack of balance that is normally provided by fission [26]. To determine if reduced Drp1 protein expression contributes to the elongated mitochondrial phenotype normally observed in A549 cells, cell lines were transfected with Drp1-YFP plasmid to overexpress Drp1-YFP fusion protein, which is functionally capable of inducing fission [16]. As shown in Figure 4A (+Drp1-YFP), Drp1 overexpression rescued the mitochondrial phenotype in A549 cells, decreasing mitochondrial lengths to those observed in basal NL20 cells (Figure 4A: mean \pm SEM; +Drp1-YFP (A6), $5.1\pm 0.7 \mu\text{m}$; 1-way ANOVA, Tukey post-test, $P>0.05$). The mitochondrial morphology of A549 cells following Drp1 overexpression similarly resembled that of basal NL20 cells (Figure 4A1). Mitochondrial length in NL20 cells (Figure 4A: mean \pm SEM; basal (A1), $4.9\pm 0.5 \mu\text{m}$) also decreased after Drp1 overexpression (Figure 4A: mean \pm SEM; +Drp1-YFP (A5), $2.1\pm 0.3 \mu\text{m}$; 1-way ANOVA, Tukey post-test, $P<0.001$).

These data suggest that a deficiency in Drp1 protein levels contributes to decreased mitochondrial fission events in A549 cells. FRAP (fluorescence recovery after photobleaching) was used to quantify mitochondrial connectivity, which infers mitochondrial fission events [16], in living NL20 and A549 cells (Figure 4E–H). FRAP curves were summarized by calculating the mobile fraction of mitochondrial-directed yellow fluorescent protein (mito-YFP), which estimates mitochondrial connectivity [16]. FRAP experiments confirm that A549 cells have decreased mitochondrial fission (Figure 4F–H). Mobile fraction values show that mitochondria in NL20 cells have significantly lower functional connectivity (more fission) when compared to A549 cells basally (Figure 4F).

Downregulation of Drp1 by overexpression of a dominant negative version of Drp1 (Drp1 K38A) equilibrated the mitochondrial connectivity between the two cell lines (Figure 4H). Following Drp1 overexpression (+Drp1-myc), mitochondrial fission is enhanced in A549 cells such that mobile fraction values are more comparable to basal NL20 cells (Figure S2). These FRAP results mimic the mitochondrial morphological observations which show decreased Drp1-dependent fission in A549 cells when compared to NL20 cells and that downregulated fission in A549 cells can be rescued by overexpression of Drp1.

Drp1 Localization in A549 Cells

To further examine decreased Drp1-dependent fission in A549 cells, we looked at Drp1 localization following subcellular fractionation via immunoblot. Mitochondrial and cytosolic fractions were examined for endogenous Drp1 protein levels (Figure 5A,B). Drp1 protein was not observed in the mitochondrial fraction of A549 cells suggesting that Drp1 is not actively recruited to the mitochondria for fission. In contrast, NL20 cells showed recruitment of Drp1 to the mitochondrial fraction, which infers mitochondrial fission is occurring in NL20 cells as suggested by the mitochondrial morphological analyses (Figure 1A, 4A) and confirmed by FRAP data (Figure 4F–H). In mammalian cells, Drp1 is recruited to the outer mitochondrial membrane following apoptotic induction [5]. To examine this translocation, Drp1 localization was visualized by immunoblot following subcellular fraction after staurosporine (STS) treatment. STS is a protein kinase inhibitor known to induce apoptosis [27]. Upon apoptotic induction by STS, Drp1 protein recruitment from the cytosolic to the mitochondrial fraction was observed in both NL20 and A549 cells (Figure 5B). From this observation, we inferred that A549 cells have decreased Drp1 mitochondrial recruitment that can be enhanced by apoptotic stimulation. This suggests that Drp1 can be recruited to the mitochondria in A549 cells but the process of mitochondrial fission is impeded in this cell line.

Impaired Cytochrome C Release in A549 Cells

Inhibiting mitochondrial fission delays the release of cytochrome c into the cytoplasm [28]; therefore, we examined

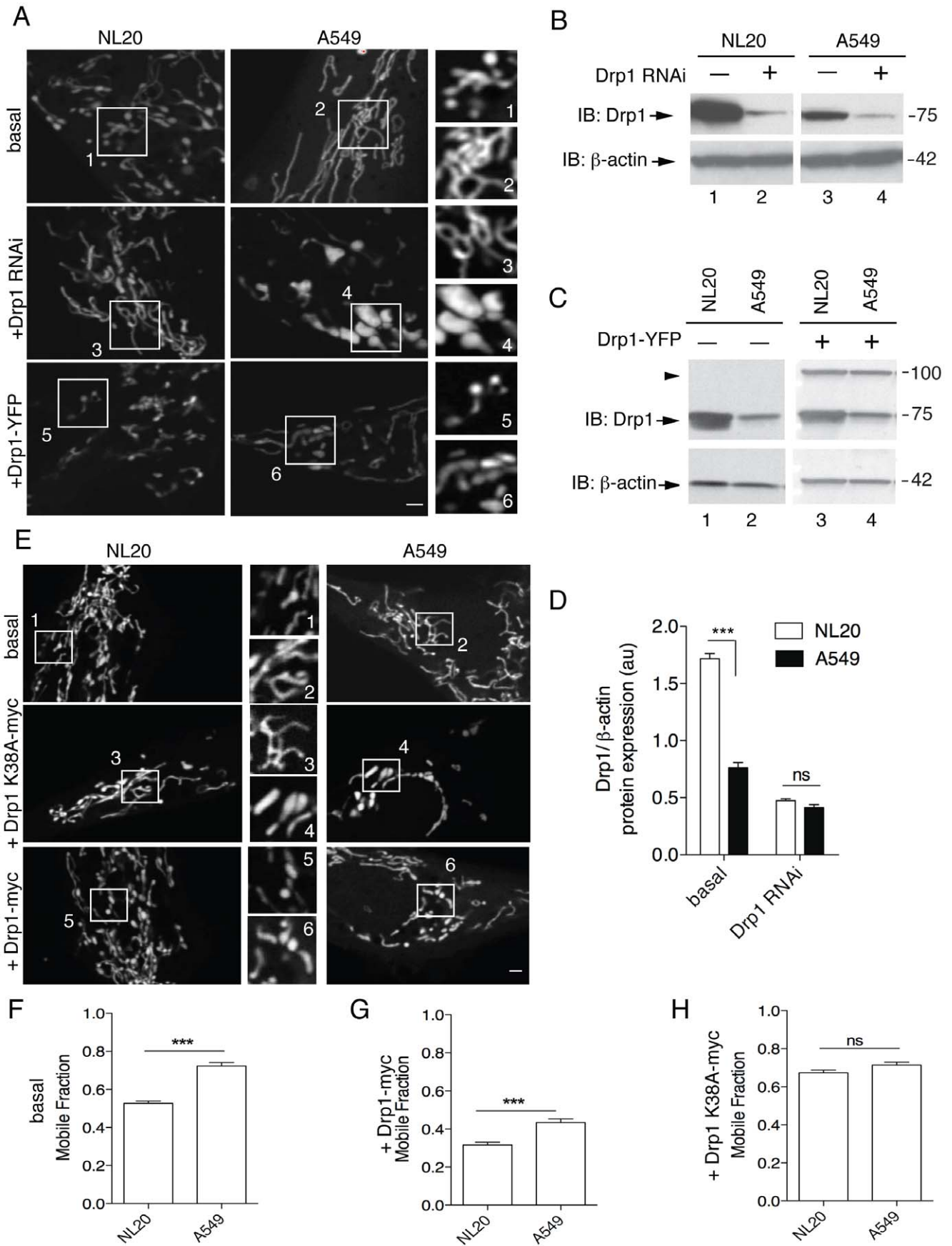
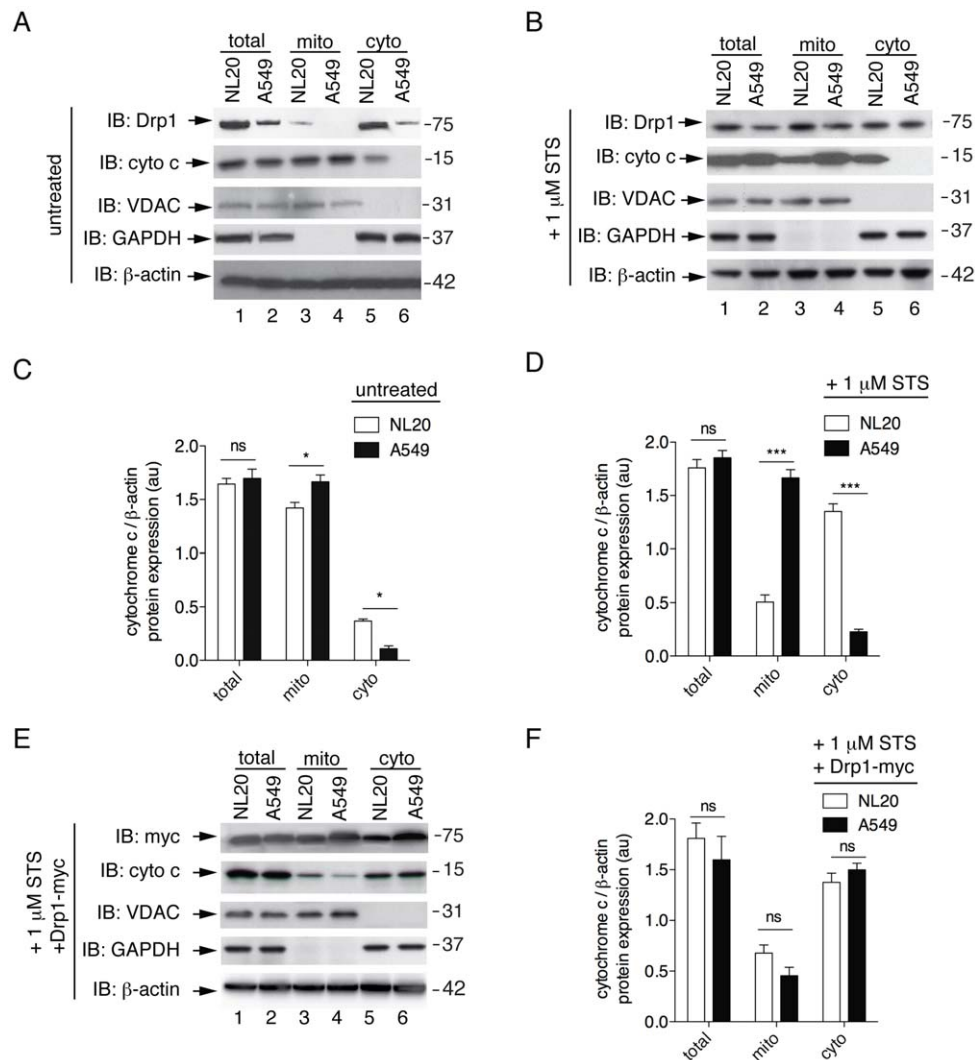


Figure 4. Decreased Drp1 protein expression and Drp1-dependent mitochondrial fission. (A) Mitochondrial morphology of NL20 (left) and A549 (right) cells following mito-DsRED transfection. Representative images shown: basal (upper) and following Drp1 RNAi (middle) or Drp1-YFP transfection (lower). The scale bar indicates 2 μ m. Numbered boxes (1–6) are magnifications (10 \times) of the corresponding numbered boxed regions in the original images. (B) Immunoblot of endogenous Drp1 expression before (lanes 1,3) and after (lanes 2,4) Drp1 RNAi transfection in NL20 and A549 cells. (C) Immunoblot of endogenous (lanes 1,2; arrow) and ectopic (lanes 3,4; arrowhead) Drp1 expression before and after Drp1-YFP transfection in NL20 and A549 cells. (B,C) β -actin reprobe to show loading; markers in kDa. (D) Relative Drp1 protein expression normalized to β -actin before and after Drp1 RNAi transfection in NL20 (white bar) and A549 (black bar) cells (two independent experiments). 2-way ANOVA analysis with Bonferroni post-tests. (E) Representative images from FRAP analysis of NL20 (left) and A549 (right) cells transfected with mito-YFP. Cells imaged under basal (top), Drp1 K38A-myc downregulation of Drp1 (middle) and Drp1-myc overexpression (bottom) conditions. Numbered boxes (1–6) are magnifications (10 \times) of the corresponding numbered boxed regions in the original images. Scale bar is 1 μ m. (F–H) Mobile fraction of mito-YFP values occurring within a single subcellular region of interest (n=60 cells). Mean and SEM shown from two independent experiments. 1-way ANOVA analysis with Tukey post-tests. Additional FRAP statistics are shown in Figure S2. doi:10.1371/journal.pone.0045319.g004

cytochrome c translocation in A549 cells (Figure 5, Figure S3). Mitochondrial and cytosolic fractions were examined for cytochrome c release in NL20, NL20TA, Calu1 and A549 cells with

and without CCCP-induced uncoupling (Figure S3A,B). Specifically, A549, the most tumorigenic cell line in this panel (Figure S1), displayed impairment in cytochrome c release following CCCP



treatment (Figure S3B,C). STS-treated A549 cells showed a similar lack of cytochrome c release when compared to NL20 cells (Figure 5B, Figure S3C). Immunoblots were quantified to show cytochrome c protein levels in fractionation experiments without and with STS-treatment (Figure 5C,D). Under basal and STS conditions, A549 cells had increased cytochrome c protein levels in the mitochondrial fraction when compared to NL20 cells. These data suggest A549 cells have decreased Drp1-dependent mitochondrial fission and the downstream process of cytochrome c release is impaired. To further support this idea, overexpression of DRP1 in A549 cells rescued STS-treatment induced release cytochrome c in this cell line (Figure 5E,F; Figure S3C) demonstrating that impaired cytochrome c release observed in A549 cells is due to a deficiency in Drp1. Expected mitochondrial morphological phenotypes were observed following STS-treatment and in combination with Drp1-myc overexpression (Figure S5), supporting the cytochrome c release immunoblot data in NL20 and A549 cells.

Apoptotic Resistance in A549 Cells

Since mitochondrial fission defects delay cytochrome c release [28] and caspase activation [5], we examined downstream pro-apoptotic events following cytochrome c release. Cleavage of caspase-3, a key mediator of mammalian apoptosis [29], was observed following STS- and doxorubicin-treatment (Figure 6A, Figure S4A,C) in NL20, NL20TA, and Calu1 cells. In contrast, caspase-3 cleavage was absent in apoptosis stimulated A549 cells (Figure 6A; Figure S4A). PARP cleavage, a downstream component of apoptosis that is caused in part by activation of caspase-3 [30], was also examined following apoptotic induction (Figure 6B, Figure S4B,D). PARP cleavage was observed in NL20 cells following apoptotic stimuli but was absent in A549 cells. Inhibition of STS-induced PARP cleavage in NL20 cells was observed upon concomitant treatment with zVAD-FMK (Figure 6C), a known caspase inhibitor, demonstrating that this is a caspase mediated process in NL20 cells. Complete PARP cleavage was observed in STS-treated NL20 cells overexpressing Drp1 protein (Figure 6C). STS-treatment induced PARP cleavage was restored in A549 cells overexpressing Drp1 (Figure 6C). These data suggest that A549 cells are resistant to apoptosis due to a downregulation of Drp1 protein expression.

Impaired Mitophagy in A549 Cells

There is a relationship between mitochondrial fission and the induction of mitochondrial selective autophagy, also known as mitophagy [31]. During mitophagy, the pre-autophagosome engulfs mitochondria to form an autophagosome. Concurrently, the cytosolic protein microtubule-associated protein 1A/1B-light chain 3 (LC3-I, 18 kDa) is conjugated to phosphatidylethanolamine to form LC3-phosphatidylethanolamine conjugate (LC3-II, 16 kDa) [32]. LC3-II is then recruited to autophagosomal membranes prior to fusion with the lysosome, which then proteolytically degrades autophagosomal internal components including LC3-II [32]. As such, lysosomal turnover of the autophagosomal marker LC3-II reflects autophagic events, such as mitochondrial selective degradation by autophagy, and detecting LC3 by immunoblotting or immunofluorescence is the standard for monitoring autophagy [11,33].

Previous studies have shown that defects in mitochondrial fission decrease mitochondrial degradation or mitophagy [11]. Autophagy was assessed by immunoblot and immunostaining (Figure 7). We monitored steady state LC3-I to LC3-II conjugation by immunoblotting for endogenous LC3 (Figure 7A) [20]. Less LC3-II conjugate was observed in untreated A549 cells when

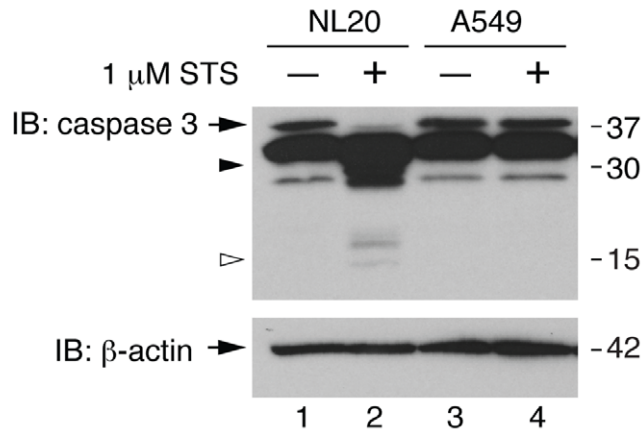
compared to NL20 cells (Figure 7B–D), which suggests basal autophagy is decreased in A549 cells relative to NL20 cells. Serum starvation, which induces autophagy, was used as a positive control. No significant difference in the amount of LC3-II following serum starvation was observed between NL20 and A549 cell lines following serum starvation (Figure 7B, EBSS), suggesting that A549 cells possess the functional capacity for autophagy. Cells were also treated with Bafilomycin A1 (BafA1), which prevents lysosomal degradation and results in the increased accumulation of LC3-II and autophagosomes [20]. NL20 cells showed efficient autophagic flux as demonstrated by the presence of more LC3-II banding than LC3-I following BafA1 treatment (Figure 7A). Because the level of LC3-II is not greater than LC3-I in BafA1 treated A549 cells, A549 does not show efficient autophagic flux and we can infer that autophagy is impaired prior to degradation by the lysosome in this cell line (Figure 7A). To further support this data an LC3 turnover assay was performed (Figure 7A; lanes 4,8), which combines serum starvation and lysosomal inhibition to monitor flux [34]. A complete turnover of LC3-II was noted in NL20 cells, whereas A549 cells had similar LC3-II expression levels as observed with only Bafilomycin treatment. These results further support autophagy being limited in A549 cells. To confirm this observation in another technique, autophagosomes were noted by the detection of LC3 punctae and mitophagy was inferred by the colocalization of LC3 punctae with mito-YFP expression using confocal microscopy (Figure 7C). A significant difference in the percentage of cells with <6 mitochondrial localized LC3 punctae was identified between basal and CCCP-treated A549 cells (Figure 7D). This observation shows that depolarization of the mitochondria after CCCP treatment does not significantly induce mitophagy in A549 cells. However, following Drp1 overexpression in A549 cells and subsequent treatment with CCCP, the percentage of cells undergoing mitophagy increased significantly (Figure 7D). These data suggest that A549 cells have impaired mitophagy.

Discussion

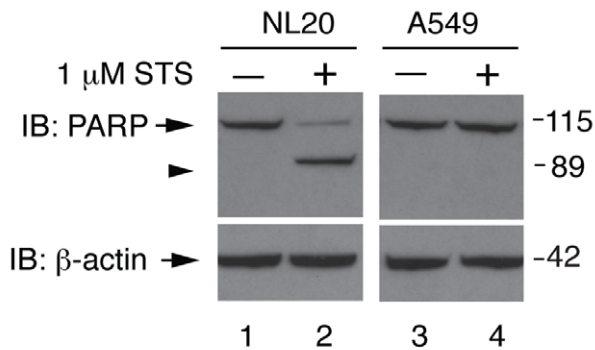
In this study, A549 cells displayed elongated mitochondrial phenotypes basally and hyperfused mitochondria following down-regulation of Drp1, consistent with phenotypes observed in cells that are deficient in mitochondrial fission [5,35]. Additional similarities to cells lacking Drp1 were noted in A549 cells, such as resistance to mitochondrial depolarization and impaired cytochrome c release from the mitochondria [5]. Drp1 activity can be altered by mitochondrial recruitment, post-translational modification and its oligomerization state [5]. This study shows decreased expression and recruitment of Drp1 to mitochondrial fractions in A549 cells relative to non-tumorigenic NL20 cells, and decreased Drp1-dependent mitochondrial fission. Drp1 associates with mitochondrial fission sites upon oligomerization [5]. Because Drp1 was observed in mitochondrial fractions following apoptotic stimuli (Figure 5C,D), we presumed Drp1 oligomerization was intact in A549 cells. To determine if phosphorylation of Drp1 was involved in the observed inhibition of mitochondrial fission in A549 cells, we examined the phosphorylation status DRP1 in both A549 and NL20 cells (Figure S6). We noted a significant increase in the phosphorylation of Drp1 in A549 cells, which would inhibit GTPase activity and subsequent fission events [5]. This phosphorylation data supports the hypothesis that A549 cells have decreased mitochondrial fission.

Defects in mitochondrial dynamics have been implicated in numerous degenerative neurological disorders [36]. The disruption of an antagonistic response by Drp1 in mitochondrial

A



B



C

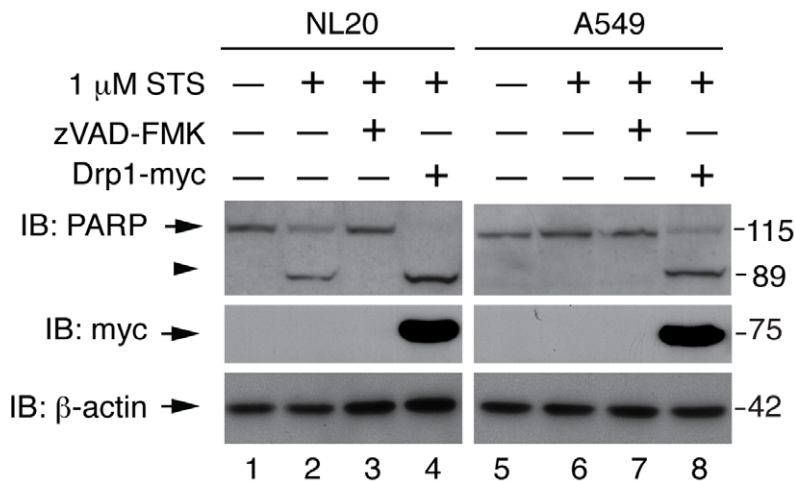
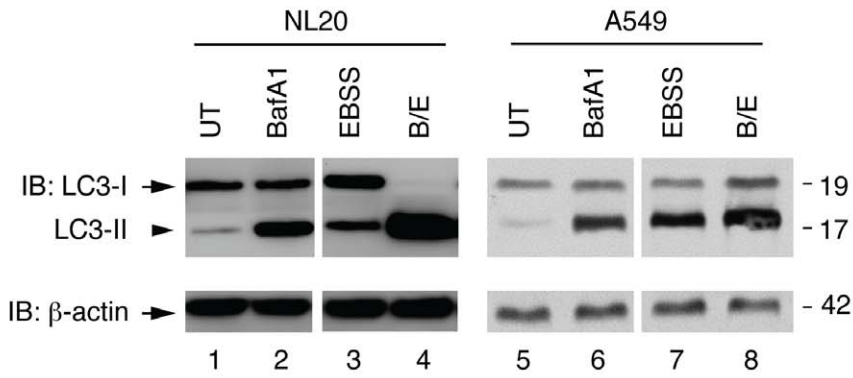
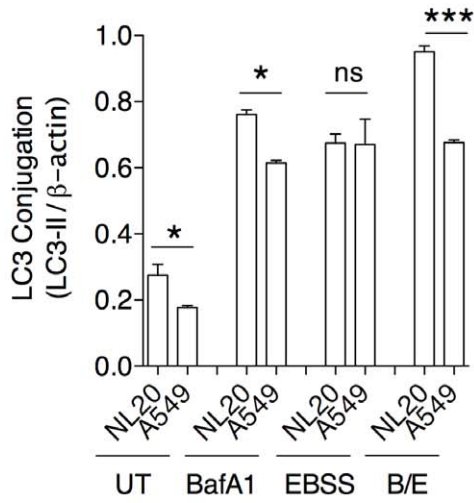


Figure 6. Resistance to STS-induced caspase-3 and PARP cleavage. (A, B) NL20 and A549 cells treated with (lanes 2,4) and without (lanes 1,3) 1 μM STS for 3 hours to induce apoptosis. β-actin reprobe to show loading. Immunoblots show (A) endogenous caspase-3 protein expression; full length (arrow) and cleaved products (open or closed arrowhead). (B) Endogenous PARP protein expression; full length (arrow) and cleaved product (arrowhead). (C) Endogenous PARP protein expression; full length (arrow) and cleaved product (arrowhead) in NL20 and A549 cells treated with 50 μM zVAD-FMK (lanes 3,7) for 4 h to inhibit caspase activity in non-transfected (lanes 1–3, 5–7) or Drp1-myc transfected (lanes 4,8) cells or co-treatment with 1 μM STS for 3 h (lanes 2–4,6–8). (A–C) Markers in kDa.
doi:10.1371/journal.pone.0045319.g006

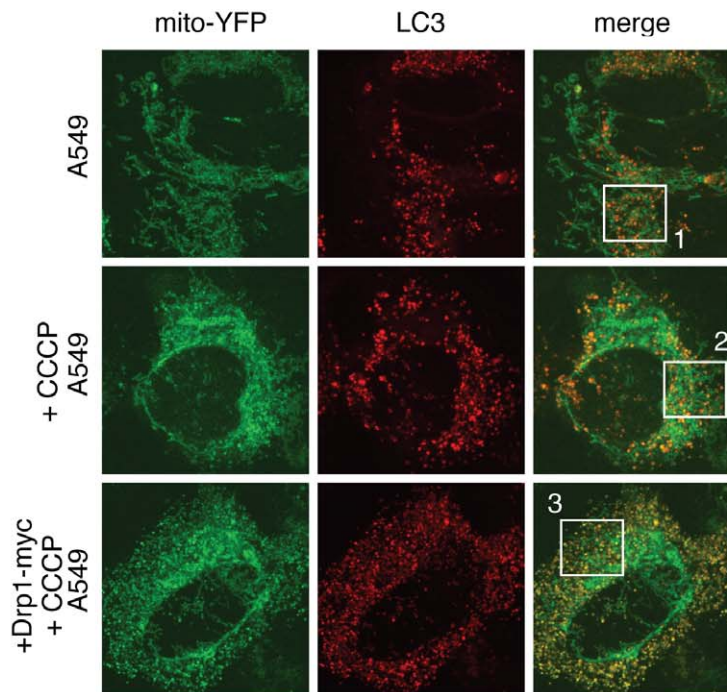
A



B



C



D

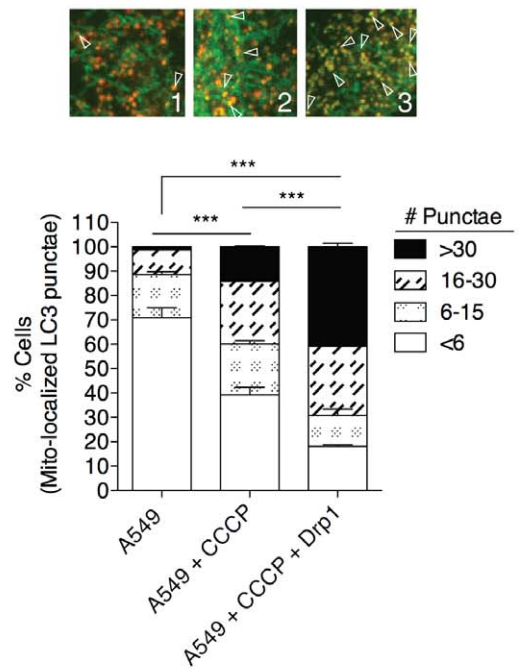


Figure 7. Impaired turnover of mitochondria prior to degradation by the lysosome. (A) Representative immunoblot of LC3-I (arrow) to LC3-II (arrowhead) conversion in total protein from untreated (UT; lanes 1,5), 10 nM 24 h Bafilomycin A1 treated (BafA1; lanes 2,6) 24 h serum starved (EBSS; lanes 3,7) or combined 24 h BafA1/EBSS treated (B/E; lanes 4,8) NL20 and A549 cells. β -actin reprobe to show loading. (B) LC3-II quantification (normalized to β -actin) from two independent experiments. Cells conditions were as in (A) to examine differences between (B) cell lines. Mean and SEM shown, 2-way ANOVA analysis with Bonferroni post-test. (C) Mito-YFP transfection (left) and LC3 immunostaining (middle) in A549 cells show mitophagy by colocalization of LC3 with the mitochondria (merged, right). A549 cells treated with 10 μ M CCCP for 30 minutes (middle) or transfected with Drp1-myc for 24 h and CCCP treated (bottom). Representative images of mitophagy by colocalization of mito-YFP and LC3 punctae (yellow expression) in CCCP and CCCP/Drp1-myc conditioned A549 cells. Scale bar is 2 μ m. (D) Quantification of mitophagy as in (C). Box insets show enlarged microscopy sections to illustrate a selection of mitophagy events occurring (white open arrowheads) which are labeled 1–3 corresponding to original images as shown in (E); A549 (1), A549+CCCP (2), and A549+CCCP/Drp1-myc (3). Percent cell counts (>200) from three independent experiments were based on colocalization of LC3 punctae staining with mito-YFP (values represent mean number of punctae counts per cell binned with SEM). 2-way ANOVA analysis with Bonferroni post-tests.
doi:10.1371/journal.pone.0045319.g007

dynamics could potentially impact many key cellular events, such as development, apoptosis, autophagy, synaptic plasticity and cell division [37]. Extensive cross-talk exists between autophagy and apoptosis [38]; in non-tumorigenic cells, the deletion of genes regulating autophagy is associated with decreased apoptosis [9]. Accordingly, alterations in apoptosis and autophagy were observed in tumorigenic A549 cells.

Efficient removal of damaged mitochondria by mitophagy requires fission of the mitochondrial network [11]. Turnover of damaged mitochondria stimulates mitochondrial biogenesis to replenish each cell with a stable pool of functional mitochondria. With respect to metabolic function, changes in mitochondrial mass can be indicative of mitochondrial proliferative potential or turnover [39]. In A549 cells, we observed an increased mitochondrial mass, which may indicate a lack of mitochondrial degradation by mitophagy [40]. We inferred defects in mitophagy by decreased LC3-II protein expression observed in A549 cells. Decreased mitophagy is influenced by Drp1 expression, as mitophagy is rescued in A549 cells following Drp1 overexpression.

Recent literature supports our findings whereby mitochondria elongate and are spared from autophagic degradation and sustain viability [41], purposing that regulated changes in mitochondrial morphology determine the fate of the cell during autophagy. As the role of autophagy in tumor progression and treatment is controversial [42], perhaps regulation of mitochondrial morphology is indeed the determinant factor in the cellular response to autophagy.

The data presented fit our hypotheses, which suggest that elongated mitochondrial lengths observed in A549 cells correlate with decreased mitochondrial fission events, and subsequent decreases in both apoptotic initiation and autophagy in this tumorigenic cell line. This work is novel in that we have identified defects in mitochondrial dynamics, namely in the mitochondrial fission mediator Drp1, which contribute to tumorigenic conversion in lung cancer cells. To summarize, tumorigenic A549 cells exhibit mitochondrial dynamic imbalances, which downregulate pro-apoptotic signaling in these tumorigenic lung epithelial cells allowing deregulated cells to survive. We also demonstrate decreased Drp1 protein expression and increased Drp1 protein phosphorylation in A549 cells, relative to the normal lung epithelial cell line NL20, which allows substandard mitochondria to accumulate causing defects in mitochondrial clearance, which potentially impacts further mitochondrial function and tumorigenesis.

Decreased Drp1 expression and activity observed in A549 cells could be due to transcriptional regulation. Drp1-dependent fission has been shown to be inhibited by miR-30 family members through suppression of its modifier, the *p53 tumor suppressor* gene [43]. It is noteworthy that A549 cells express the wild-type version of *p53* [44] and p53 protein expression in these cells is not statistically different from NL20 cells (data not shown). In addition

to post-transcriptional gene silencing, other RNA polymerase modifiers may be regulating Drp1 gene transcription and subsequent activity.

Other possible hypotheses of Drp1 regulation include further post-translational modifications. As we have inferred, like others have demonstrated [45,46], Drp1 mediated fission is negatively regulated by phosphorylation. Drp1 function has also been shown to be modulated in part by calcineurin-dependent dephosphorylation [16]. Tumorigenic A549 cells could potentially have decreased phosphatase enzymatic activity or constitutively active Drp1 phosphorylation, both of which would limit GTP-dependent mitochondrial fission. Moreover, sumoylation of Drp1 has been shown to positively regulate its activity and mitochondrial morphology [47,48]. Downregulation of sumoylation players may also putatively inhibit mitochondrial fission in tumorigenic cells. Drp1 is also modified by ubiquitination [5], a process that targets the protein for destruction. This modification could potentially influence the turnover of Drp1, which might explain the significant decrease in protein expression observed in A549 cells when compared to controls.

Future studies in A549 cells will examine the influence of Drp1 modifiers including the cristae-remodeling pathway, controlled in part by Opa1, on the downstream processes of mitochondrial dynamics, autophagy and apoptosis in tumorigenic lung epithelial cells.

Supporting Information

Figure S1 Tumorigenic potential measured by cell migration assay. Percent cell migration was assessed in NL20, NL20TA, Calu1 and A549 cells using a standard Boyden chamber assay. Mean and SEM shown from triplicate (n = 8 cell measurements) experiments. 1 way ANOVA analysis with Tukey post-tests compared to NL20 cells ($P < 0.0001$). (TIF)

Figure S2 Additional FRAP analysis. Mobile fraction of mito-YFP values in NL20 and A549 cells are displayed which estimate mitochondrial connectivity or the relative amount of mitochondrial fission that is occurring in a single region of interest within the cell under basal, Drp1 K38A-myc downregulation or Drp1-myc overexpression. Mean and SEM shown from duplicate (n = 60 cell measurement) experiments. 1-way ANOVA analysis with Tukey post-tests. (TIF)

Figure S3 Cytochrome c release following mitochondrial uncoupling. (A,B) NL20 (lanes 1–3), NL20TA (lanes 4–6), Calu1 (lanes 7–9), and A549 (lanes 10–12) cells were harvested and subcellular fractionation was performed to examine mitochondrial and cytosolic fractions. Total (T: lanes 1,4,7,10), mitochondrial (M: lanes 2,5,8,11) and cytosolic (C: lanes 3,6,9,12) lysates were immunoblotted for endogenous cytochrome c. The mitochondrial

(VDAC) and cytosol (GAPDH) markers and β -actin are shown as loading and fractionation controls. Markers are in kDa. (B) Cells were treated with 10 μ M CCCP for 1 h to induce mitochondrial decoupling to examine cytochrome c release. (C) NL20 (left panels) and A549 (right panels) cells were transfected with mito-dsRED and immunostained for cytochrome c to show mitochondrial (red/orange) or cytoplasmic (green) localization. Colocalization of mitochondria and cytochrome c is indicated by yellow. Cells were untreated (top panels), treated with 1 μ M STS for 3 h (second panels), treated with 10 μ M CCCP for 1 h (third panels), co-transfected with Drp1-myc (fourth panels) or co-transfected with Drp1-myc and treated with 1 μ M STS for 3 h (bottom panels). Scale bar is 2 μ m. (TIF)

Figure S4 Apoptotic stimulus in epithelial cells. (A,B) NL20 (lanes 1,3) and A549 (lanes 2,4) cells untreated (lanes 1,2) or treated for 24 h with 1 μ g/ml doxorubicin (lanes 3,4). β -actin reprobe to show loading. (C,D) NL20TA (lanes 1,2) and Calu1 (lanes 3,4) cells untreated (lanes 1,3) or treated for 3 h with 1 μ M STS (lanes 2,4). NL20TA (lanes 5,6) and Calu1 (lanes 7,8) cells untreated (lanes 5,7) or treated for 24 h with 1 μ g/ml doxorubicin (lanes 6,8). β -actin reprobe to show loading. (A,C) Immunoblots show endogenous caspase 3 protein expression (full length, arrow; cleaved products, open or closed arrowhead). (B,D) Immunoblots show endogenous PARP protein expression (full length, arrow; cleaved products, arrowhead). (A–D) Markers in kDa. (TIF)

Figure S5 Mitochondrial morphology following STS exposure. (A) Mitochondrial morphology of NL20 (left panels) and A549 (right panels) cells following mito-YFP transfection.

References

- Ryang DY, Joo YE, Chung KM, Lim SR, Jeong HK, et al. (2007) Expression of c-FLIP in gastric cancer and its relation to tumor cell proliferation and apoptosis. *Korean J Intern Med* 22: 263–269.
- Glinksy GV, Glinksy VV, Ivanova AB, Hueser CJ (1997) Apoptosis and metastasis: increased apoptosis resistance of metastatic cancer cells is associated with the profound deficiency of apoptosis execution mechanisms. *Cancer Lett* 115: 185–193.
- Fulda S, Galluzzi L, Kroemer G (2010) Targeting mitochondria for cancer therapy. *Nat Rev Drug Discov* 9: 447–464.
- Shivapurkar N, Reddy J, Chaudhary PM, Gazdar AF (2003) Apoptosis and lung cancer: a review. *J Cell Biochem* 88: 885–898.
- Suen DF, Norris KL, Youle RJ (2008) Mitochondrial dynamics and apoptosis. *Genes Dev* 22: 1577–1590.
- Rosignol R, Gilkerson R, Aggeler R, Yamagata K, Remington SJ, et al. (2004) Energy substrate modulates mitochondrial structure and oxidative capacity in cancer cells. *Cancer Res* 64: 985–993.
- Youle RJ, Karbowski M (2005) Mitochondrial fission in apoptosis. *Nat Rev Mol Cell Biol* 6: 657–663.
- Chen H, Chan DC (2005) Emerging functions of mammalian mitochondrial fusion and fission. *Hum Mol Genet* 14 Spec No.2: R283–289.
- Boya P, Gonzalez-Polo RA, Casares N, Perfettini JL, Dessen P, et al. (2005) Inhibition of macroautophagy triggers apoptosis. *Mol Cell Biol* 25: 1025–1040.
- Estaquier J, Arnould D (2007) Inhibiting Drp1-mediated mitochondrial fission selectively prevents the release of cytochrome c during apoptosis. *Cell Death Differ* 14: 1086–1094.
- Twig G, Elorza A, Molina AJ, Mohamed H, Wikstrom JD, et al. (2008) Fission and selective fusion govern mitochondrial segregation and elimination by autophagy. *Embo J* 27: 433–446.
- Tan ML, Ooi JP, Ismail N, Moad AI, Muhammad TS (2009) Programmed cell death pathways and current antitumor targets. *Pharm Res* 26: 1547–1560.
- Lee HK, Jones RT, Myers RA, Marzella L (1992) Regulation of protein degradation in normal and transformed human bronchial epithelial cells in culture. *Arch Biochem Biophys* 296: 271–278.
- Balsara BR, Pei J, Mitsuuchi Y, Page R, Klein-Szanto A, et al. (2004) Frequent activation of AKT in non-small cell lung carcinomas and preneoplastic bronchial lesions. *Carcinogenesis* 25: 2053–2059.
- Kim KW, Hwang M, Moretti L, Jaboin JJ, Cha YI, et al. (2008) Autophagy upregulation by inhibitors of caspase-3 and mTOR enhances radiotherapy in a mouse model of lung cancer. *Autophagy* 4: 659–668.
- Sandebring A, Thomas KJ, Beilina A, van der Brug M, Cleland MM, et al. (2009) Mitochondrial alterations in PINK1 deficient cells are influenced by calcineurin-dependent dephosphorylation of dynamin-related protein 1. *PLoS One* 4: e5701.
- Frank S, Gaume B, Bergmann-Leitner ES, Leitner WW, Robert EG, et al. (2001) The role of dynamin-related protein 1, a mediator of mitochondrial fission, in apoptosis. *Dev Cell* 1: 515–525.
- Smirnova E, Shurland DL, Ryazantsev SN, van der Bliek AM (1998) A human dynamin-related protein controls the distribution of mitochondria. *J Cell Biol* 143: 351–358.
- Lee YJ, Jeong SY, Karbowski M, Smith CL, Youle RJ (2004) Roles of the mammalian mitochondrial fission and fusion mediators Fis1, Drp1, and Opa1 in apoptosis. *Mol Biol Cell* 15: 5001–5011.
- Thomas KJ, McCoy MK, Blackinton J, Beilina A, van der Brug M, et al. (2011) DJ-1 acts in parallel to the PINK1/parkin pathway to control mitochondrial function and autophagy. *Hum Mol Genet* 20: 40–50.
- Krebiel G, Ruckerbauer S, Burbulla LF, Kieper N, Maurer B, et al. (2010) Reduced basal autophagy and impaired mitochondrial dynamics due to loss of Parkinson's disease-associated protein DJ-1. *PLoS One* 5: e9367.
- Bellance N, Lestienne P, Rosignol R (2009) Mitochondria: from bioenergetics to the metabolic regulation of carcinogenesis. *Front Biosci* 14: 4015–4034.
- Ayyasamy V, Owens KM, Desouki MM, Liang P, Bakin A, et al. (2011) Cellular model of Warburg effect identifies tumor promoting function of UCP2 in breast cancer and its suppression by genipin. *PLoS One* 6: e24792.
- Agnello M, Morici G, Rinaldi AM (2008) A method for measuring mitochondrial mass and activity. *Cytotechnology* 56: 145–149.
- Petit PX, Goubern M, Dirole P, Susin SA, Zamzami N, et al. (1998) Disruption of the outer mitochondrial membrane as a result of large amplitude swelling: the impact of irreversible permeability transition. *FEBS Lett* 426: 111–116.
- Autret A, Martin SJ (2010) Bcl-2 family proteins and mitochondrial fission/fusion dynamics. *Cell Mol Life Sci* 67: 1599–1606.
- Wang C, Youle RJ (2009) The role of mitochondria in apoptosis*. *Annu Rev Genet* 43: 95–118.
- Cassidy-Stone A, Chipuk JE, Ingerman E, Song C, Yoo C, et al. (2008) Chemical inhibition of the mitochondrial division dynamin reveals its role in Bax/Bak-dependent mitochondrial outer membrane permeabilization. *Dev Cell* 14: 193–204.
- Lakhani SA, Masud A, Kuida K, Porter GA, Jr., Booth CJ, et al. (2006) Caspases 3 and 7: key mediators of mitochondrial events of apoptosis. *Science* 311: 847–851.

Representative images shown: basal (upper panels), and following 3 h treatment with 1 μ M STS (middle panels) or Drp1-myc co-transfection with 3 h 1 μ M STS treatment (lower panels). The scale bar indicates 2 μ m. Box insets (numbered 1–6) to the far right are magnified (10 \times) regions corresponding to the numbered boxes in the original images.

(TIF)

Figure S6 Analysis of Drp1 phosphorylation. (A) Cell lysates from NL20 and A549 cells were separated by phospho-enrichment (P; lanes 1,3) and compared to total lysates (T; lanes 2,4). With immunoblot, endogenous Drp1 was found in both phospho- and total fractions. Immunoblotting for Drp1 pSer637 was also included. Controls for purification include immunoblotting for non-phosphorylated HSP60 and phosphorylated HTRA2. Markers in kDa. (B) The ratio of phospho- to total Drp1 was quantified (B) from two independent experiments between the two cell lines. Mean and SEM shown. T-test analysis ($P=0.0071$). (TIF)

Acknowledgments

Thanks to Richard Youle and Megan Cleland for plasmids and the NINDS imaging core, which allowed KJT to perform FRAP experiments. We would also like to thank Marcel P. van der Brug and Susan F. Radka for critical reading of the manuscript.

Author Contributions

Conceived and designed the experiments: KJT. Performed the experiments: KJT. Analyzed the data: KJT MRJ. Contributed reagents/materials/analysis tools: KJT. Wrote the paper: KJT.

30. Boulares AH, Yakovlev AG, Ivanova V, Stoica BA, Wang G, et al. (1999) Role of poly(ADP-ribose) polymerase (PARP) cleavage in apoptosis. Caspase 3-resistant PARP mutant increases rates of apoptosis in transfected cells. *J Biol Chem* 274: 22932–22940.
31. Twig G, Shirihai OS (2011) The interplay between mitochondrial dynamics and mitophagy. *Antioxid Redox Signal* 14: 1939–1951.
32. Tanida I, Ueno T, Kominami E (2004) LC3 conjugation system in mammalian autophagy. *Int J Biochem Cell Biol* 36: 2503–2518.
33. Klionsky DJ, Abeliovich H, Agostinis P, Agrawal DK, Aliev G, et al. (2008) Guidelines for the use and interpretation of assays for monitoring autophagy in higher eukaryotes. *Autophagy* 4: 151–175.
34. Mizushima N, Yoshimori T, Levine B (2010) Methods in mammalian autophagy research. *Cell* 140: 313–326.
35. Mopert K, Hajek P, Frank S, Chen C, Kaufmann J, et al. (2009) Loss of Drp1 function alters OPA1 processing and changes mitochondrial membrane organization. *Exp Cell Res* 315: 2165–2180.
36. Chen H, Chan DC (2009) Mitochondrial dynamics—fusion, fission, movement, and mitophagy—in neurodegenerative diseases. *Hum Mol Genet* 18: R169–176.
37. Chang CR, Blackstone C (2010) Dynamic regulation of mitochondrial fission through modification of the dynamin-related protein Drp1. *Ann N Y Acad Sci* 1201: 34–39.
38. Maiuri MC, Zalckvar E, Kimchi A, Kroemer G (2007) Self-eating and self-killing: crosstalk between autophagy and apoptosis. *Nat Rev Mol Cell Biol* 8: 741–752.
39. Narendra DP, Jin SM, Tanaka A, Suen DF, Gautier CA, et al. (2010) PINK1 is selectively stabilized on impaired mitochondria to activate Parkin. *PLoS Biol* 8: e1000298.
40. Rodriguez-Enriquez S (2009) Roles of mitophagy and the mitochondrial permeability transition in remodeling of cultured rat hepatocytes. *Autophagy* 5.
41. Gomes LC, Di Benedetto G, Scorrano L (2011) During autophagy mitochondria elongate, are spared from degradation and sustain cell viability. *Nat Cell Biol* 13: 589–598.
42. Kimmelman AC (2011) The dynamic nature of autophagy in cancer. *Genes Dev* 25: 1999–2010.
43. Li J, Donath S, Li Y, Qin D, Prabhakar BS, et al. (2010) miR-30 regulates mitochondrial fission through targeting p53 and the dynamin-related protein-1 pathway. *PLoS Genet* 6: e1000795.
44. Lehman TA, Bennett WP, Metcalf RA, Welsh JA, Ecker J, et al. (1991) p53 mutations, ras mutations, and p53-heat shock 70 protein complexes in human lung carcinoma cell lines. *Cancer Res* 51: 4090–4096.
45. Cribbs JT, Strack S (2007) Reversible phosphorylation of Drp1 by cyclic AMP-dependent protein kinase and calcineurin regulates mitochondrial fission and cell death. *EMBO Rep* 8: 939–944.
46. Chang CR, Blackstone C (2007) Cyclic AMP-dependent protein kinase phosphorylation of Drp1 regulates its GTPase activity and mitochondrial morphology. *J Biol Chem* 282: 21583–21587.
47. Harder Z, Zunino R, McBride H (2004) Sumo1 conjugates mitochondrial substrates and participates in mitochondrial fission. *Curr Biol* 14: 340–345.
48. Zunino R, Schauss A, Rippstein P, Andrade-Navarro M, McBride HM (2007) The SUMO protease SENP5 is required to maintain mitochondrial morphology and function. *J Cell Sci* 120: 1178–1188.
49. Schiller JH, Bitner G, Wu SQ, Meisner L (1998) Karyotypic changes associated with spontaneous acquisition and loss of tumorigenicity in a human transformed bronchial epithelial cell line: evidence for in vivo selection of transformed clones. *In Vitro Cell Dev Biol Anim* 34: 283–289.
50. Momiki S, Baba M, Caamano J, Iizasa T, Nakajima M, et al. (1991) In vivo and in vitro invasiveness of human lung carcinoma cell lines. *Invasion Metastasis* 11: 66–75.
51. Satoh H, Lamb PW, Dong JT, Everitt J, Boreiko C, et al. (1993) Suppression of tumorigenicity of A549 lung adenocarcinoma cells by human chromosomes 3 and 11 introduced via microcell-mediated chromosome transfer. *Mol Carcinog* 7: 157–164.